Ternary-Responsive Field-Effect Transistors and Multilevel Memories Based on Asymmetrically Functionalized Janus Few-Layer WSe2

Haixin Qiu, Martin Herder, Stefan Hecht, Paolo Samorì

WILEY-VCH

Ternary-Responsive Field-Effect Transistors and Multilevel Memories Based on Asymmetrically Functionalized Janus Few-Layer WSe_2

*Haixin Qiu, Martin Herder, Stefan Hecht, Paolo Samorì**

H. Qiu, Prof. P. Samorì

University of Strasbourg, CNRS, ISIS UMR 7006, 8 Allée Gaspard Monge, F-67000 Strasbourg, France.

Email: samori@unistra.fr

Dr. M. Herder, Prof. S. Hecht

Department of Chemistry and IRIS Adlershof, Humboldt-Universität zu Berlin, 12489, Berlin.

Prof. S. Hecht

Germany, DWI - Leibniz Institute for Interactive Materials, Forckenbeckstr. 50, 52074 Aachen, Germany, & Institute of Technical and Macromolecular Chemistry, RWTH Aachen University, Worringer Weg 2, 52074 Aachen, Germany.

Keywords: 2D semiconductors, multi-stimuli-responsive transistors, photochromic, ferroelectric, high-density memories

Abstract

Hybrids composed of two-dimensional (2D) transition metal dichalcogenides with stimuli-responsive molecules are prototypical components for the development of multifunctional field-effect transistors (FETs), whose output currents can be remotely controlled by external inputs. Herein, ternary-responsive FETs based on few-layer WSe_2 are realized by decorating the two opposite surfaces of the 2D semiconductor with different stimuli-responsive molecules in an asymmetric fashion: the bottom surface is interfaced with a photochromic diarylethene film and the top surface with a ferroelectric poly(vinylidene fluoride–trifluoroethylene) layer. Such novel Janus ternary device architecture shows superior functional complexity compared with normal mono-stimuli-responsive FETs. The synergy between the two molecularly induced effects enables the devices to respond orthogonally to electric field and light irradiation, with an enhanced output current modulation efficiency of 87%. The 9 ferroelectric and 84 photo-generated states ensure 756 current levels in a single device. The over 10 cycles of cyclic endurance and more than 1000 hours of retention time confirm the reliability of each state, implementing the demand for high-density non-volatile memories, as well as enriching the diversification in “More than Moore” technologies.

1. Introduction

The emerging "More than Moore" technologies, which are characterized by integrating novel analog functionalities within semiconductor-based devices, bring vast diversification rather than pure miniaturization to CMOS digital circuitry.[1] The integration of molecular components into digital circuits has been demonstrated to be a powerful strategy to endow functional diversification, taking advantage of the almost infinite variety of molecules that can be synthesized.[2] Towards this end, stimuli-responsive molecules are particularly interesting because of their capacity to be interconverted between two or more states, having markedly distinct properties when subjected to external stimuli such as electromagnetic, electric or magnetic fields or changes in the environment (pH, temperature, etc.).[3] By incorporating such molecules in a conventional field-effect transistor (FET), novel stimuli-responsive capacity can be imparted to the device thereby enabling to manipulate their electrical output by means of various external inputs. Such approach is instrumental for various applications in advanced electronic devices such as memories,[4] sensors[5] and smart logic gates.[6]

Recent efforts have been dedicated to the fabrication of stimuli-responsive devices based on two-dimensional (2D) transition metal dichalcogenides (TMDs), which are atomically thin semiconductors possessing extraordinary electronic properties compared to their organic counterparts.[7] Possessing unique physico-chemical characteristics, TMDs have been employed as promising channel material in low-power and high-performance digital electronic switches.[8] Moreover, due to their high surface-to-volume ratio, monolayer and few-layer TMDs have an exquisite surface sensitivity to any subtle surrounding environmental change, which opens up the opportunity to modify their intrinsic properties.[9] Recent studies involving stimuli-responsive molecules to decorate the surface of TMDs demonstrated this approach as a promising strategy to non-destructively modulate the charge carrier density by translating the stimuli-triggered changes at the molecular level to the modification of TMD's properties without introducing any defect.[10]

Among the possible external stimuli, light and electrical inputs are particularly interesting since they are efficient, non-invasive, and spatiotemporally precise. Photochromic molecules are optically responsive systems able to undergo reversible photoisomerization when irradiated with light at specific wavelengths.[11] Hitherto they have been utilized as optical switching elements to translate photonic information into electrical output in TMD-based FETs.[12] We recently reported a proof of this concept by exploiting tailor-designed photochromic diarylethene (DAE) molecules to reversibly tune the charge carrier transport in few-layer WSe_2 and demonstrated a potential application of the corresponding FET as optically switchable multilevel non-volatile memory.[12a, 12b]

On the other hand, ferroelectric materials have been employed to precisely control the doping level of 2D materials.[13] According to the direction of the external electric field, their intrinsic bistable polarization can be reoriented, leading to an accumulation or depletion of the charge carriers in the interfaced semiconducting material.[14] Interestingly, these ferroelectric field-effect transistors (FeFETs) take advantage of the binary remnant polarization states of the ferroelectric to store information and therefore have successfully been utilized in practical non-volatile memories.[15]

To date, multifarious molecularly functionalized 2D-mono-stimuli-responsive FETs have been reported, in which direct deposition of functional molecules on top of the upper channel surface served as effective and easily addressable approach to fabricate the device.[16] The inversed device structure could also be obtained by first depositing the molecules on a suitable substrate, followed by transfer of the 2D materials.[17] In all the previous studies only one face of the 2D materials was functionalized by molecules and thus a potential asymmetry arising from unequal exposure of the two surfaces to two different local environments was not exploited. Such a scenario can be achieved by the independent functionalization of each surface with a different functional molecule,[18] providing intriguing perspectives for the realization of multi-stimuli-responsive FETs.

Along these lines, here we report an unprecedented approach based on the decoration of few-layer WSe_2 flakes with two different stimuli-responsive (macro)molecules thereby generating a Janus 2D material. In particular, the bottom surface was sitting on a light-responsive DAE layer and the top surface was coated with an electrically responsive copolymer layer of poly(vinylidene fluoride–trifluoroethylene) (P(VDF-TrFE)). In this way, a multi-stimuli-responsive FET has been fabricated in which the output current could be reversibly and precisely modulated by means of either light irradiation or an electric field. Note that in order to largely preserve the intrinsic electrical properties of WSe_2 and enable a reversible remote-control of its charge carrier transport, the less invasive physisorption approach was employed. Compared with conventional mono-stimuli-responsive FETs, our novel ternary device architecture combines enhanced functional complexity with fabrication simplicity. We provide unambiguous evidence for the compatibility of the device response to both optical and electrical stimuli, thereby offering an orthogonal handle for operating the device, which is beneficial for memory applications as well. By taking advantage of the synergic effect between the two (macro)molecular switches, the device has attained an enhanced modulation of the output current with an efficiency reaching up to 87%. Furthermore, with each stimulus manifesting a large number of different outputs without mutual interferences (9 electric-induced levels and 84 light-induced levels), the device yields a total number of 756 distinct states, outperforming the current state-of-the-art mono-stimuli-responsive transistors thereby providing a decisive step forward to address the demand for high-density storage memories.[12a, 19] The reliability of each state is further reflected by the endurance and retention tests for 5 arbitrary states, exhibiting a notable endurance for over 10 cycles and an excellent data retention exceeding 1000 hours. Moreover, compared with cumbersome synthesis of single molecules incorporating different functional groups to realize the multi-addressable elements,[20] our Janus modified ternary structure relies on a simple fabrication process and appears to be a universal strategy

that can be extended to other 2D materials and functional molecules, offering a versatile platform for the construction of multi-stimuli-responsive devices.

2. Mechanism and device fabrication

The photoisomerization of DAE molecules between ring-open DAE_O and ring-closed DAE_C form is accompanied by a major change in their corresponding energy levels.[21] By taking advantage of this unique characteristic, a DAE derivative has been designed and synthesized to possess well-defined lowest unoccupied molecular orbital (LUMO) energy levels in the two states (**Figure 1a**) with respect to the conduction band of WSe_2 thereby exhibiting two different and reversible regimes of charge transfer upon light irradiation. In particular, the LUMO level of DAE_O lies higher than the conduction band minimum of WSe_2 which blocks electron transfer from the latter. On the contrary, the LUMO level of DAE_C lies comfortably below the conduction band minimum of WSe_2 and thus significant electron trapping is expected.[22] In other words, in view of such reciprocal energy levels, electron transfer from WSe_2 to DAE_C is foreseeable by UV irradiation, and trapped electrons can get restored in WSe_2 by subsequent vis irradiation. Figure 1b portrays the architecture of the DAE/WSe_2/FeFET device. A layer of DAE molecules was first spin-coated to the pre-cleaned Si/SiO_2 substrate. Then, mechanically exfoliated few-layer WSe_2 flakes were transferred onto the SiO_2 substrates previously coated with DAE. The source and drain electrodes were deposited lithography-free via metal evaporation (60 nm Au) through a shadow mask, which not only protects the DAE layer from being removed during the lift-off process but also avoids contamination by photoresist residues. With the underlying physisorbed DAE layer guaranteeing the light responsive capacity, the top surface of WSe_2 is ready for being interfaced with the ferroelectric P(VDF-TrFE) layer to impart the ferroelectric responsive nature. The P(VDF-TrFE) layer was transferred on the top of the DAE/WSe_2 device via a wet transfer approach (Figure S1). Note that direct spin-coating of P(VDF-TrFE) solution onto the DAE/WSe_2 chip is avoided since the solvent (methylethylketone) would remove DAE

molecules, and moreover, the formation of P(VDF-TrFE) film requires curing at 140 °C for 2 hours to increase its crystallinity, which may deteriorate the switching capacity of the DAE molecules.[23]

3. Results and discussions

The photomodulation effect induced by DAE molecules was first examined in a DAE/WSe_2 FET. As displayed in Figure S6, the initial device reveals a typical n-type dominant behavior with electron mobility of 13.8 $cm^2V^{-1}s^{-1}$. Upon subsequent exposure to UV or vis light, the electron current could be reversibly modulated with an efficiency of 74%. Such value is even higher than the one obtained for the inverse heterostructure, *i.e.* WSe_2 coated with a top DAE layer.[12b] The improved efficiency is attributed to a better interface contact between the DAE and WSe_2 layers.

To cast light onto the ferroelectric properties of P(VDF-TrFE) polymer, it was integrated as the dielectric material into a capacitor. Figure 1c shows the typical hysteresis loops for a P(VDF-TrFE) capacitor with the thickness of 500 nm. The coercive electric field appears at ≈ 0.9 $MVcm^{-1}$ (corresponding to a coercive voltage of 38 V) and the remnant polarization value is ≈ 7.3 μCcm^{-2}, indicating a good quality of the P(VDF-TrFE) film.[24] The measurement cycle was repeated 10 times to gain insight into the ferroelectric stability and no fatigue was observed.

Regarding the DAE/WSe_2/FeFET device, its transfer characteristics were first investigated in back gate configuration, which showed a typical n-type dominant behavior with an electron mobility of 18.2 $cm^2V^{-1}s^{-1}$ (Figure S7a, black curve). The enhanced mobility compared with DAE/WSe_2 device by adding P(VDF-TrFE) as top gate is correlated to its high dielectric constant (ε_r = 10), which suppresses the Coulomb scattering in the WSe_2 channel.[25] Next, the electrical performance of the same device was characterized in top gate configuration with P(VDF-TrFE) serving as the dielectric. As the top gate voltage (V_{tg}) sweeps between –60 V and +60 V (Figure 1d, blue curve), the transfer curve shows a large memory hysteresis window (≈ 45 V). The generation of such memory window is entirely related to the polarization

switching process of the P(VDF-TrFE). The state of the P(VDF-TrFE) can be programmed by the top gate bias: The positive voltage exceeding its coercive voltage can polarize the ferroelectric into the downward direction P_{down}. With the positively charged C-H bond facing the WSe_2 channel, electrons in the WSe_2 will be engaged to compensate for the polarization charges. Conversely, the application of a negative voltage exceeding the coercive voltage will induce a polarization of the P(VDF-TrFE) into the upward direction P_{up}. In this case, with the negatively charged C-F bond facing the channel, the compensation charge converts from electrons to holes, leading to a depletion of electrons in the channel. Moreover, the corresponding gate leakage current I_{tg} exhibits two apparent peaks near the coercive voltage, which further proves the polarization behavior of the P(VDF-TrFE) (Figure 1d, red curve). The polarization remains stable during the measured 10 cycles, proving the retained dielectric and ferroelectric properties of the P(VDF-TrFE). The electron mobility derived from the top gate configuration is 32.3 $cm^2V^{-1}s^{-1}$. Due to the better dielectric shielding effect of P(VDF-TrFE) compared to SiO_2,[26] the value is much higher than that obtained from the back gate configuration.

Subsequently, the electrical and optical switching capacity of the device was examined. For electrical switching, the electrical characteristics of WSe_2 were detected from the back gate configuration after programming the P(VDF-TrFE) into different states by applying a top gate bias exceeding its coercive voltage (±60 V). Figure S7a shows a representative transfer evolution cycle. In the P_{down} state, an increase of the electron current can be observed accompanied with a negative shift of the threshold voltage. In contrast, in the P_{up} state, the electron current decreased when compared to the initial state, with a modulation efficiency of 68% at a back gate voltage V_{bg} = 60 V (as compared with the P_{down} state). The corresponding threshold voltage moved in the positive direction. At the same time, an increase of the hole current was observed and the device showed an electron-dominant ambipolar behavior. Such effective current modulation triggered by P(VDF-TrFE) proves the electrical switching

capacity of the device. We next explored the optical switching capacity rooted by DAE molecules. As presented in Figure S7c, the current photomodulation efficiency is largely preserved compared with DAE/WSe_2 FET, which slightly decreases from 74% to 59%, suggesting that the wet transfer process does not significantly diminish the light responsive property of DAE molecules.

In an effort to demonstrate that the device can respond synergistically to light irradiation and an electric field, the two stimuli were incorporated to switch the device. In **Figure 2a**, the starting point was the state possessing the highest current level: **S1-1** P_{down}/DAE_O. The device was first exposed to UV light to switch the DAE molecules from their ring-open to their ring-closed form. With some electrons trapped by the ring-closed isomer, a decrease of the current was observed, and the device reached a second state **S1-0**: P_{down}/DAE_C. Next, the polarization direction of the polymer was switched from downward to upward by applying a negative top gate bias (–60 V). This process further depleted the electrons in the channel and the device thereof reached its lowest current level, corresponding to a third state **S0-0**: P_{up}/DAE_C. Subsequently, vis light was used to switch the DAE molecules back to their ring-open form. In the channel, the trapped electrons were released, and the current was partially recovered, reaching a fourth state **S0-1**: P_{up}/DAE_O. Ultimately, by applying a positive gate bias (+60 V), the P(VDF-TrFE) was switched to downward direction, electrons would again be accumulated, promoting the full recovery of the current and the device returned back to the original state **S1-1**. This reversible current modulation behavior provides unambiguous evidence that the optical switching can be incorporated in an orthogonal manner with the electrical switching.

Aiming at verifying the compatibility between the two stimuli, we further recorded the transfer evolution by reversing the stimuli sequences. Figure S8 shows that the 4 distinct states generated above can be freely addressed independently of the stimuli order, *i.e.,* **S0-0** P_{up}/DAE_C can be acquired from **S1-1** P_{down}/DAE_O by 2 routes: UV irradiation + negative bias and negative bias + UV irradiation. This phenomenon demonstrated the absence of mutual

interference between the light irradiation and electric field, providing evidence for the full compatibility of the electric-responsive P(VDF-TrFE) polymer with the photo-responsive DAE molecules. Figure 2b plots the normalized current modulation efficiency during the 4 switching cycles in Figure 2a and S8. In view of the synergic effect between these two molecular building blocks, the total electron current modulation efficiency reaches up to 87%. The 4 states were found to be stable during the measured cycles with different order of applied stimuli, confirming a good stability and reversibility of both electrical and optical modulation.

The switching behavior was furthermore elucidated by tracking the real time current dynamics under repeated voltage and illumination operation. In Figure 2c, the I_{ds} current at V_{bg} = 60 V in back gate configuration was collected under cyclic ±60 V pulses applied to the top gate (each cycle contains 2 s +60 V, blue boxed region; 30 s 0 V; 2 s -60 V, violet boxed region; 30 s 0 V, enlarged single cycle was shown in Figure S9a). The measurement started from the current state with the ferroelectric polymer in the upward direction. The device was first triggered by a +60 V pulse. In response to such transient voltage pulse, a current spike appears with the amplitude up to ~ 1.5 μA. When the bias was reset to 0 V, instead of resuming to the original state, the current ramps to a higher value and stays constant at that state, indicating the switch of the ferroelectric polymer into downward direction. Conversely, in response to a symmetric negative pulse –60 V, the current declines back to the lower level and holds stable at that value. Under such successive cycles of ±60 V pulses, the device switched steadily between the generated two states. The current behavior at V_{bg} = 0 V modulated by periodic UV/vis illumination is shown in Figure 2d (each cycle contains 5 s UV, orange boxed region; 20 s dark; 20 s vis, green boxed region; 20 s dark, enlarged single cycle was shown in Figure S9b). When the illumination was switched on, there was a surge of the current, which is attributed to the photogenerated electron-hole pairs. As the DAE isomerization progressed, the current presented a gradual decrease during UV illumination, due to the continuous trapping of electrons by photogenerated DAE_C. After the UV illumination was terminated, the current

exhibited a lower value, and such reduced current could recover progressively by subsequent vis illumination. At the end of the illumination cycle, the current level resumed to the pre-irradiation value, in good accordance with the results obtained from the transfer measurements. In a control experiment, WSe_2/FeFET without DAE molecules was tested under the same illumination conditions, exhibiting only photoresponse yet no modulation behavior (Figure S10). Moreover, for both electrical and optical switching, the absence of degradation over 20 consecutive cycles confirms the durability and robustness of the device, which are crucial prerequisites for memory applications.

Since both electrical and optical modulation display a high effiency, the suitability of our FET device as a multibit memory can be envisaged. Upon adjusting the population ratio between P_{up} and P_{down}, which can be controlled by the applied top gate voltage, intermediate ferroelectric current levels can be obtained between these two saturated states during the P(VDF-TrFE) polarization process.[27] Similarly, by tuning the population ratio between $DAE\__O$ and $DAE\__C$, which can be controlled by the light exposure, multiple photogenerated current levels can be achieved accordingly.[12a] In order to fulfill the demand of high-density storage in practical memory applications, the maximum number of levels that can be achieved by each stimulus have been investigated.

Figure 3a depicts the transfer evolution from **S1-1** to **S0-1** programmed by various top gate sweeps from positive to negative direction. Note that the device was kept isolated from UV/vis illumination to ensure DAE molecules would not be disturbed. The dependence of I_{ds} at V_{bg} = 60 V in back gate configuration on the programmed top gate voltage was summarized in Figure 3b which shows a continuous decrease after each step-increasing sweep and generates in a total number of 9 clear storage states. As the polarization of P(VDF-TrFE) does not follow a linear relationship with the applied electric field, different gaps between the applied voltage were utilized. At the sweeping range near the coercive voltage, the current varies significantly due to the efficient switch of the ferroelectric. Conversely, when the range exceeds the coercive

voltage, the current decreases slowly due to the saturation of the channel. Hence, a larger gap (10 V) between the applied voltage is utilized at the beginning and at end, while a smaller gap (1 V) is utilized near the coercive voltage. More states can be defined if the applied bias gap was reduced, but the value variation of each generated state during repeated cycles could in turn increased. Therefore, in order to guarantee the reproducibility of generated states, we defined only 9 storage states. Note that the electron current evolution behavior remains the same under different back gate bias, as clearly demonstrated in Figure S11a. Likewise, starting from **S0-1** and applying the sweep in the opposite direction from negative to positive, the current level can increase stepwise and restore to **S1-1** (Figure S11b-d). In order to demonstrate that such multilevel behavior is independent of the DAE state, another four pairs were chosen: **S0-0**/**S1-0** when DAE molecules are in their ring-closed form, and **S0-0.55/S1-0.55**, **S0-0.35/S1-0.35, S0-0.15/S1-0.15** when DAE molecules are at an arbitrary state with both ring-open and ring-closed forms. As presented in Figure S12-S14, the current exhibited the similar evolution trend and 9 distinct levels were obtained for each pair. The results imply that multilevel data storage can be achieved by precisely controlling the programming top gate voltage.

When it comes to optical switching, starting from **S1-1**, the device was exposed to a periodic short time UV pulses. The corresponding dynamic current behavior was displayed in Figure 3c, with enlarged regions in Figure 3d. Note that in order to eliminate the gate bias stress effect, we applied 0 V to the back gate during the measurement.[28] The current decreased progressively after each light dose, proving a continual electron depletion from the WSe_2 channel. Totally 84 UV doses were employed, enabling to reach 84 current states with the final saturation state corresponding to **S1-0**. The clear current difference between each two neighbouring levels proves the validity of each state. As previously demonstrated, 9 ferroelectric states can be generated at each fixed DAE state. Therefore, with 84 photogenerated levels, the device can ideally yield a maximum number of 756 current levels, corresponding to a memory with a data storage capacity exceeding 9 bit.

In order to prove such prediction, Figure 3e illustrates the multilevel current achieved by controlling both electric field and light illumination during 5 cycles between **S1-1** and **S0-0**. In the first cycle, in the absence of a contribution from P(VDF-TrFE), the current between **S1-1** and **S1-0** was divided into 5 well-defined levels by illumination with different time of UV dose:10 s **S1-0.55**, 20 s **S1-0.35**, 40 s **S1-0.15** and 80 s **S1-0**. Then at **S1-0**, the device went a step further by switching the P(VDF-TrFE) into P_{up} direction, arriving at the final state **S0-0**. The stored optical and electrical information can be erased by vis irradiation and positive bias, restoring to **S1-1**. In the following cycles, the P(VDF-TrFE) switching step was inserted during DAE switching process. Notably, we found that the polymer switching is accessible from any photo generated interstate and yields 4 new states: **S0-0.15**, **S0-0.35**, **S0-0.55** and **S0-1**, confirming our preliminary prediction that the device possesses the unequivocal data storage exceeding 9 bit. Moreover, the interstate obtained by different routes held stable values with negligible standard deviation, proving an accurate readout (Table S1).

The reliability of the multilevel memory was demonstrated by both cyclic endurance and retention time tests. Apart from the full ON **S1-1** and OFF **S0-0** state, 3 arbitrary states were chosen: **S1-0.35**, **S0.5-0.35** and **S0-0.35**. The endurance test was performed under cyclic voltage/illumination operations: Starting from **S1-1**, the following states were obtained by applying 30 s UV → ±39 V sweep → –60 V pulse → 120 s UV in sequence, and **S1-1** could be reobtained by 10 min vis + +60 V pulse. **Figure 4a** profiles the drain current at V_{bg} = 60 V for these 5 states during 10 cycles. Interestingly, we observed only a minor fluctuation for each state and no deterioration, indicating that each programmed current level is highly reproducible. By taking advantage of the excellent fatigue resistance from both DAE and P(VDF-TrFE),[13a, 29] our DAE/WSe_2/FeFET possesses the potential of a notable endurance with more cycles. The retention property for each state was evaluated by independently monitoring the current as a function of storage time. It is worth noting that the device is kept without perturbation of electric field and illumination. As illustrated in Figure 4b, P(VDF-TrFE) fully polarized states (**S1-1**,

S1-0.35, **S0-0.35**, **S0-0**) were steadily maintained for over 1000 hours with negligible degradation, whereas **S0.5-0.35** shows a weak deterioration with a slight increase of current ~0.2 μA. Note that the reading operation by probing the source-drain voltage may locally perturbs the dipole alignment of the ferroelectric layer, resulting in a lowering of the ferroelectric polarization. Therefore, an increase of current was observed in **S0.5-0.35** due to its less robust nature and suffers from the depolarization.[30] In general, the device shows reliable non-volatile characteristics. The observed robust cyclic endurance and excellent retention time is promising for application of our DAE/WSe_2/FeFET as a high-density non-volatile memory.

4. Conclusion

In summary, by unprecedentedly interfacing 2D semiconductors with both light and ferroelectric-responsive components, we have demonstrated the operation of a multi-stimuli-responsive WSe_2 FET device. By harnessing reversible isomerization of DAE molecules and the polarization of P(VDF-TrFE) polymer, the device could respond orthogonally to light irradiation and an electric field. We observed a synergetic effect between the two stimuli, with total absence of mutual interference, yielding to an overall modulation of the output current up to 87%. Such current modulation was found being robust for over 20 cycles without perceptible attenuation. Significantly, we could achieve 9 distinguishable ferroelectric states and 84 photogenerated states, yielding to as many as 756 current levels storage in a single device. In addition, by taking full advantage of the bistability of both DAE molecules and P(VDF-TrFE) polymer, the devices demonstrated an excellent performance in cyclic endurance (10 cycles) and data retention (over 1000 hours), paving the way for their application as high-density non-volatile memories. This novel ternary Janus device architecture is generally applicable to other 2D materials and stimuli-responsive molecules, thereby opening new opportunities for next-generation multi-stimuli-responsive electronics and promoting the development of "More than Moore" technologies by enriching diversification.

Experimental Section

Experimental details are available in the Supporting Information.

Supporting Information

Supporting Information is available from the Wiley Online Library or from the author.

Acknowledgements

We acknowledge funding from the European Commission through the ERC projects SUPRA2DMAT (GA-833707) and Light4Function (GA-308117), the Graphene Flagship Core 3 project (GA- 881603), the Agence Nationale de la Recherche through the Labex projects CSC (ANR-10-LABX-0026 CSC) and NIE (ANR-11-LABX-0058 NIE) within the Investissement d'Avenir program (ANR-10-120 IDEX-0002-02), the International Center for Frontier Research in Chemistry (icFRC), the Institut Universitaire de France (IUF), the German Research Foundation (DFG via SFB 658, project B8) as well as the Chinese Scholarship Council.

Received: ((will be filled in by the editorial staff))
Revised: ((will be filled in by the editorial staff))
Published online: ((will be filled in by the editorial staff))

References

[1] a) M. M. Waldrop, *Nature News* **2016**, *530*, 144; b) T. N. Theis, H.-S. P. Wong, *Comput. Sci. Eng.* **2017**, *19*, 41; c) M. M. Waldrop, *Nature* **2016**, *530*, 144.

[2] a) M. Gobbi, E. Orgiu, P. Samorì, *Adv. Mater.* **2018**, *30*, 1706103; b) S. Bertolazzi, M. Gobbi, Y. Zhao, C. Backes, P. Samorì, *Chem. Soc. Rev.* **2018**, *47*, 6845.

[3] a) C. Simão, M. Mas-Torrent, N. Crivillers, V. Lloveras, J. M. Artés, P. Gorostiza, J. Veciana, C. Rovira, *Nat. Chem.* **2011**, *3*, 359; b) M. E. Itkis, X. Chi, A. W. Cordes, R. C. Haddon, *Science* **2002**, *296*, 1443.

[4] a) Y. Liu, Y. Yang, D. Shi, M. Xiao, L. Jiang, J. Tian, G. Zhang, Z. Liu, X. Zhang, D. Zhang, *Adv. Mater.* **2019**, *31*, 1902576; b) T. Leydecker, M. Herder, E. Pavlica, G. Bratina, S. Hecht, E. Orgiu, P. Samorì, *Nat. Nanotechnol.* **2016**, *11*, 769.

[5] a) A. Shadman, E. Rahman, Q. D. M. Khosru, *Sens Bio-sensing Res.* **2016**, *11*, 45; b) J. Liu, Y. Lu, *J. Am. Chem. Soc.* **2005**, *127*, 12677.

[6] a) P. Zhang, D. Gao, K. An, Q. Shen, C. Wang, Y. Zhang, X. Pan, X. Chen, Y. Lyv, C. Cui, *Nat. Chem.* **2020**, *12*, 381; b) X. Zhang, S. Soh, *Adv. Mater.* **2017**, *29*, 1606483.

[7] a) Q. Zhang, J. Zhang, S. Wan, W. Wang, L. Fu, *Adv. Funct. Mater.* **2018**, *28*, 1802500; b) R. Zhou, S. Zhu, L. Gong, Y. Fu, Z. Gu, Y. Zhao, *J. Mater. Chem. B* **2019**, *7*, 2588.

[8] a) M. Chhowalla, H. S. Shin, G. Eda, L.-J. Li, K. P. Loh, H. Zhang, *Nat. Chem.* **2013**, *5*, 263; b) S. Manzeli, D. Ovchinnikov, D. Pasquier, O. V. Yazyev, A. Kis, *Nat. Rev. Mater.* **2017**, *2*, 17033; c) X. Duan, C. Wang, A. Pan, R. Yu, X. Duan, *Chem. Soc. Rev.* **2015**, *44*, 8859.

[9] a) L. Yang, K. Majumdar, H. Liu, Y. Du, H. Wu, M. Hatzistergos, P. Hung, R. Tieckelmann, W. Tsai, C. Hobbs, *Nano Lett.* **2014**, *14*, 6275; b) D. M. Sim, M. Kim, S. Yim, M.-J. Choi, J. Choi, S. Yoo, Y. S. Jung, *ACS Nano* **2015**, *9*, 12115; c) S. Bertolazzi, S. Bonacchi, G. Nan, A. Pershin, D. Beljonne, P. Samorì, *Adv. Mater.* **2017**, *29*, 1606760.

[10] a) Y. Zhao, S. Bertolazzi, M. S. Maglione, C. Rovira, M. Mas-Torrent, P. Samorì, *Adv. Mater.* **2020**, *32*, 2000740; b) S. Wang, L. Tan, P. Liang, T. Liu, J. Wang, C. Fu, J. Yu, J. Dou, H. Li, X. Meng, *J. Mater. Chem. B* **2016**, *4*, 2133; c) L. Chen, X. Zhou, W. Nie, W. Feng, Q. Zhang, W. Wang, Y. Zhang, Z. Chen, P. Huang, C. He, *ACS Appl. Mater. Interfaces* **2017**, *9*, 17786.

[11] L. Wang, Q. Li, *Chem. Soc. Rev.* **2018**, *47*, 1044.

[12] a) H. Qiu, Z. Liu, Y. Yao, M. Herder, S. Hecht, P. Samorì, *Adv. Mater.* **2020**, *32*, 1907903; b) H. Qiu, Y. Zhao, Z. Liu, M. Herder, S. Hecht, P. Samorì, *Adv. Mater.* **2019**, *31*, 1903402; c) M. Gobbi, S. Bonacchi, J. X. Lian, A. Vercouter, S. Bertolazzi, B. Zyska, M. Timpel, R. Tatti, Y. Olivier, S. Hecht, M. V. Nardi, D. Beljonne, E. Orgiu, P. Samorì, *Nat. Commun.* **2018**, *9*, 2661.

[13] a) C. Zhou, Y. Chai, *Adv. Electron. Mater.* **2017**, *3*, 1600400; b) X. Chen, X. Han, Q.-D. Shen, *Adv. Electron. Mater.* **2017**, *3*, 1600460.

[14] a) Y. T. Lee, D. K. Hwang, S. Im, *J. Korean Phys. Soc.* **2015**, *67*, 1499; b) X. Wang, P. Wang, J. Wang, W. Hu, X. Zhou, N. Guo, H. Huang, S. Sun, H. Shen, T. Lin, M. Tang, L. Liao, A. Jiang, J. Sun, X. Meng, X. Chen, W. Lu, J. Chu, *Adv. Mater.* **2015**, *27*, 6575; c) D. Li, X. Wang, Y. Chen, S. Zhu, F. Gong, G. Wu, C. Meng, L. Liu, L. Wang, T. Lin, S. Sun, H. Shen, X. Wang, W. Hu, J. Wang, J. Sun, X. Meng, J. Chu, *Nanotechnology* **2018**, *29*, 105202.

[15] a) R. C. G. Naber, K. Asadi, P. W. M. Blom, D. M. de Leeuw, B. de Boer, *Adv. Mater.* **2010**, *22*, 933; b) K. Asadi, D. M. De Leeuw, B. De Boer, P. W. Blom, *Nat. Mater.* **2008**, *7*, 547.

[16] a) A. Tarasov, S. Zhang, M.-Y. Tsai, P. M. Campbell, S. Graham, S. Barlow, S. R. Marder, E. M. Vogel, *Adv. Mater.* **2015**, *27*, 1175; b) D. Kiriya, M. Tosun, P. Zhao, J. S. Kang, A. Javey, *J. Am. Chem. Soc.* **2014**, *136*, 7853.

[17] a) Y. Li, C.-Y. Xu, P. Hu, L. Zhen, *ACS Nano* **2013**, *7*, 7795; b) S. Najmaei, X. Zou, D. Er, J. Li, Z. Jin, W. Gao, Q. Zhang, S. Park, L. Ge, S. Lei, J. Kono, V. B. Shenoy, B. I. Yakobson, A. George, P. M. Ajayan, J. Lou, *Nano Lett.* **2014**, *14*, 1354.

[18] M.-A. Stoeckel, M. Gobbi, T. Leydecker, Y. Wang, M. Eredia, S. Bonacchi, R. Verucchi, M. Timpel, M. V. Nardi, E. Orgiu, P. Samorì, *ACS Nano* **2019**, *13*, 11613.

[19] H. S. Lee, S.-W. Min, M. K. Park, Y. T. Lee, P. J. Jeon, J. H. Kim, S. Ryu, S. Im, *Small* **2012**, *8*, 3111.

[20] a) F. Tian, D. Jiao, F. Biedermann, O. A. Scherman, *Nat. Commun.* **2012**, *3*, 1207; b) F. Meng, Y.-M. Hervault, Q. Shao, B. Hu, L. Norel, S. Rigaut, X. Chen, *Nat. Commun.* **2014**, *5*, 3023; c) X. Xia, H. Yu, L. Wang, Z. ul-Abdin, *RSC Advances* **2016**, *6*, 105296.

[21] M. Herder, F. Eisenreich, A. Bonasera, A. Grafl, L. Grubert, M. Pätzel, J. Schwarz, S. Hecht, *Chem. Eur. J.* **2017**, *23*, 3743.

[22] a) K. Börjesson, M. Herder, L. Grubert, D. Duong, A. Salleo, S. Hecht, E. Orgiu, P. Samorì, *J. Mater. Chem. C* **2015**, *3*, 4156; b) Y. Guo, J. Robertson, *Appl. Phys. Lett.* **2016**, *108*, 233104.

[23] M. Carroli, D. T. Duong, E. Buchaca-Domingo, A. Liscio, K. Börjesson, M. Herder, V. Palermo, S. Hecht, N. Stingelin, A. Salleo, E. Orgiu, P. Samorì, *Adv. Funct. Mater.* **2020**, *30*, 1907507.

[24] S. Liu, I. Grinberg, A. M. Rappe, *Nature* **2016**, *534*, 360.

[25] D. Jena, A. J. P. r. l. Konar, *Phys. Rev. Lett.* **2007**, *98*, 136805.

[26] B. Radisavljevic, A. Radenovic, J. Brivio, V. Giacometti, A. Kis, *Nat. Nanotechnol.* **2011**, *6*, 147.

[27] a) S. K. Hwang, I. Bae, R. H. Kim, C. Park, *Adv. Mater.* **2012**, *24*, 5910; b) M. Xu, X. Zhang, S. Li, T. Xu, W. Xie, W. Wang, *J. Mater. Chem. C* **2019**, *7*, 13477.

[28] K. Cho, W. Park, J. Park, H. Jeong, J. Jang, T.-Y. Kim, W.-K. Hong, S. Hong, T. Lee, *ACS Nano* **2013**, *7*, 7751.

[29] M. Herder, B. M. Schmidt, L. Grubert, M. Pätzel, J. Schwarz, S. Hecht, *J. Am. Chem. Soc.* **2015**, *137*, 2738.

[30] a) P. K. Larsen, R. Cuppens, G. A. C. M. Spierings, *Ferroelectrics* **1992**, *128*, 265; b) J. Lee, A. J. J. M. van Breemen, V. Khikhlovskyi, M. Kemerink, R. A. J. Janssen, G. H. Gelinck, *Sci. Rep.* **2016**, *6*, 24407.

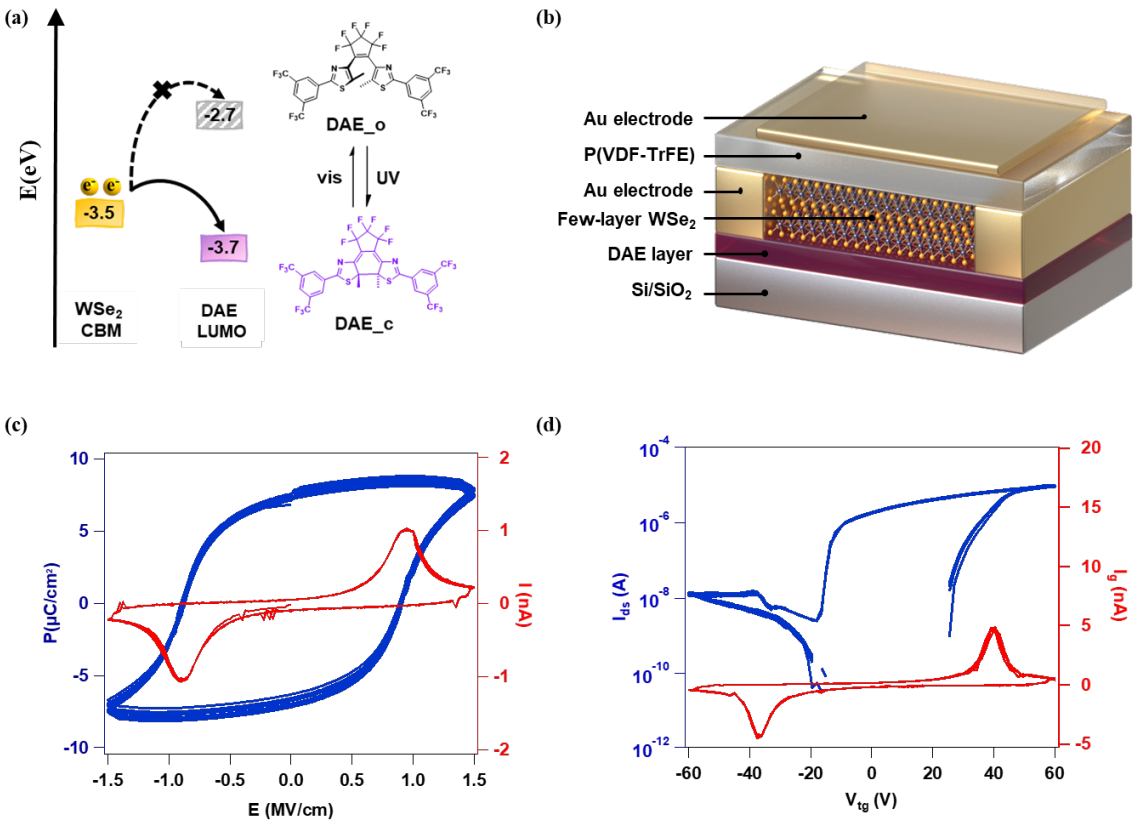

Figure 1: Energy level diagram between DAE and WSe_2, device geometry, and electrical characterization of P(VDF-TrFE) capacitor and DAE/WSe_2/FeFET. a) Energy level diagram of the electron transport between DAE/WSe_2 and the chemical structures of investigated DAE molecules. Energy level values for WSe_2 are calculated in the screened exchange functional, and the values for DAEs are measured by cyclic voltammetry. b) Schematic diagram of the DAE/WSe_2/FeFET device with double-sided decoration: the bottom surface with DAE film and the top surface with P(VDF-TrFE) layer. c) The ferroelectric hysteresis loop of a 500 nm P(VDF-TrFE) capacitor during 10 cycles. P stands for polarization, and E stands for electric filed. d) Transfer curve of a DAE/WSe_2/FeFET in top gate configuration in logarithm scale during 10 cycles (blue curve) and corresponding leakage current (red curve).

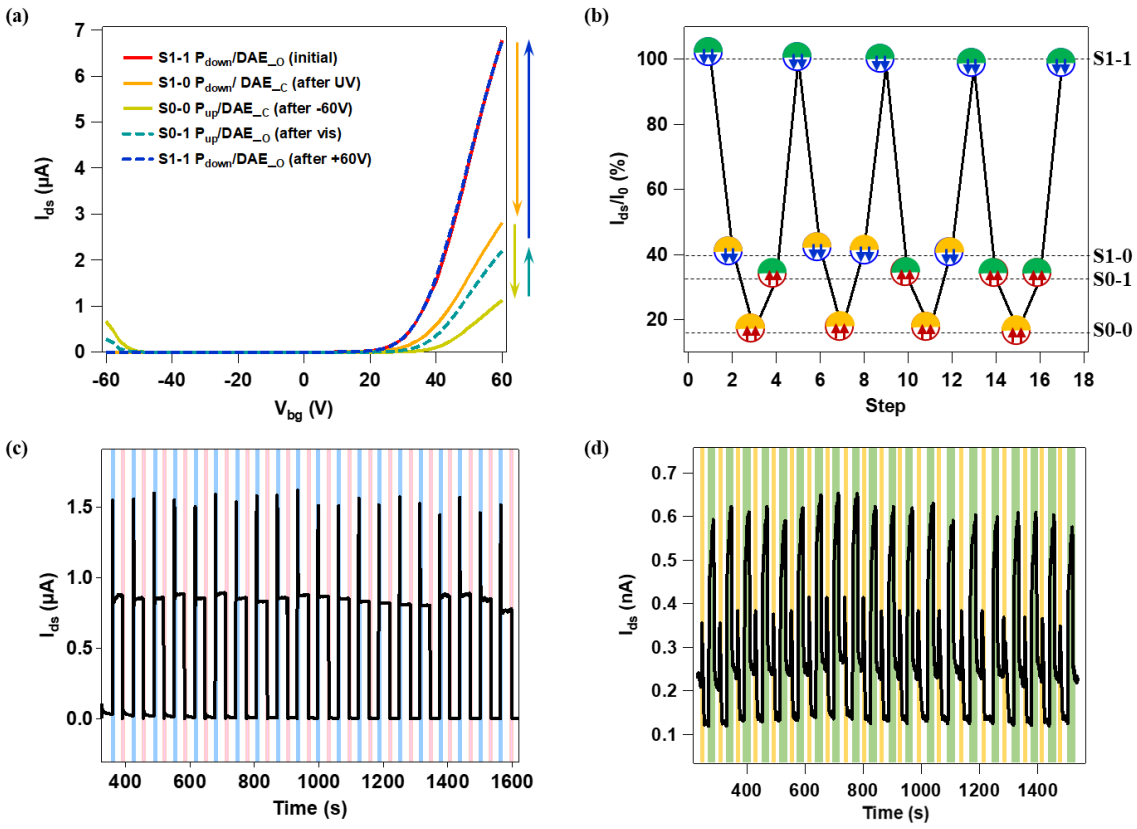

Figure 2: Orthogonally optical and electrical switching of DAE/WSe_2/FeFET. a) Transfer evolution by alternative UV/vis irradiation and ±60 V bias. b) Current modulation efficiency at V_{bg} = 60 V during the 4 switching cycles with different stimuli orders. c, d) Dynamic I_{ds} current switching behavior during 20 cycles induced by applying alternating (c) V_{tg} pulses of ±60 V and (d) UV/vis illumination.

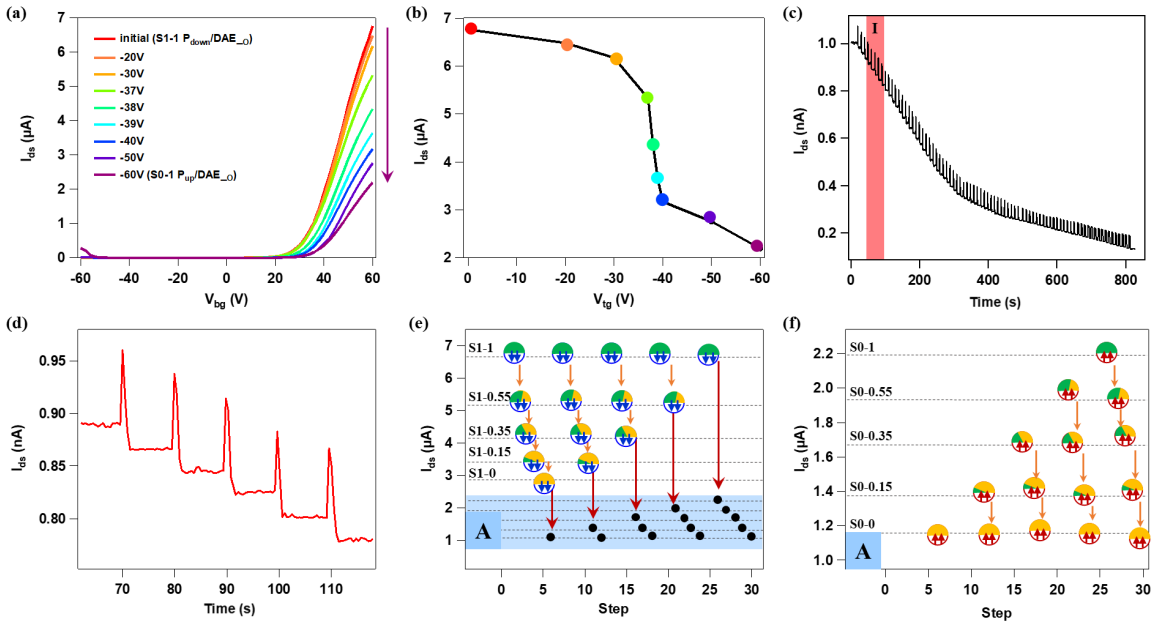

Figure 3: Multilevel storage of DAE/WSe_2/FeFET. a) Transfer evolution when partially polarizing the P(VDF-TrFE) from downward to upward direction by sweeping top gate at various ranges. b) Corresponding I_{ds} current evolution behavior at V_{bg} = 60 V as a function of programmed sweep. c, d) Dynamic I_{ds} current evolution behavior under exposure of short UV pulses at V_{bg} = 0 V: (c) totally obtained 84 levels and (d) enlarged 5 levels in region I. e) Multilevel current over five cycles by different stimuli orders. f) Enlarged levels in region A.

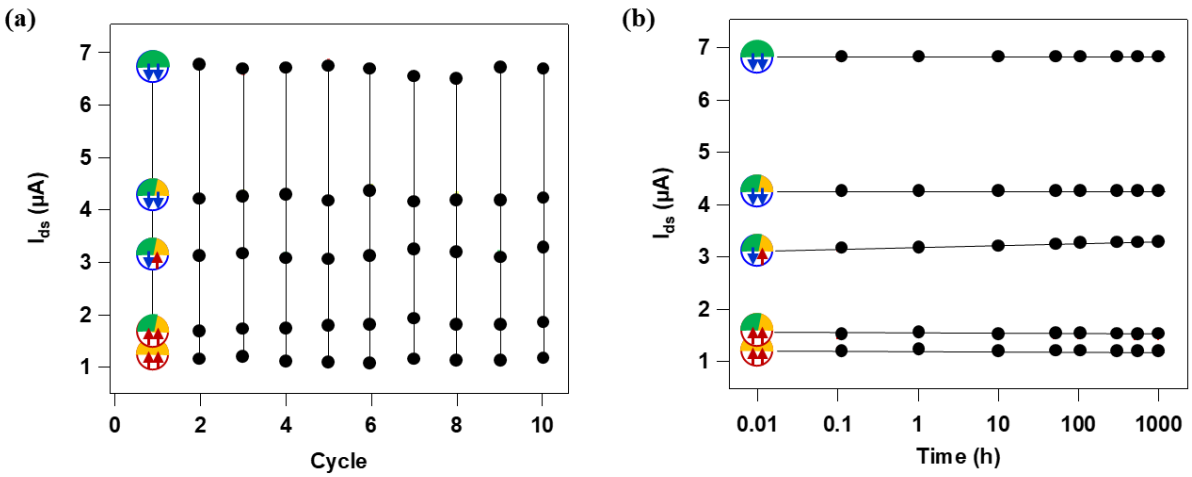

Figure 4: Memory characteristics of DAE/WSe_2/FeFET. a) Endurance performance of 5 chosen states during 10 voltage/illumination cycles. b) Time dependent retention characteristics of the 5 states.